XLI CILAMCE
XLI Ibero-Latin American Congress on Computational Methods in Engineering
16-19 November, 2020 FOZ DO IGUAÇU PARANÁ – BRAZIL

POST-FAILURE SIMULATION OF LAZY-WAVE RISERS

Beatriz M. Meneses[1], Ricardo A. de Sousa[1], Leonardo G. Ribeiro[1], Evandro Parente Jr.[1], A. Macário C. de Melo[1], Fábio P. S. Mineiro[2], Mariana T. C. G. Carneseca[2]

[1]*Laboratório de Mecânica Computacional e Visualização (LMCV), Departamento de Engenharia Estrutural e Construção Civil, Universidade Federal do Ceará*
Campus do Pici, Bloco 728, 60440-900, Ceará-Brazil
biamm98@gmail.com, ricardosousa@alu.ufc.br, leonardoribeiro@alu.ufc.br, evandro@ufc.br, macario@ufc.br
[2]*Centro de Pesquisas Leopoldo Américo Miguez de Mello (CENPES), Petrobrás*
Av. Horácio Macedo, 950, Cidade Universitária da Universidade Federal do Rio de Janeiro, Rio de Janeiro, 21941-915, Brazil
fabiomineiro@petrobras.com.br, mariana.teixeira@petrobras.com.br

Abstract. Even with great advances in methods for analysis and design of marine risers, structures still fail, resulting in their rupture and fall on the seabed. The fall can cause high environmental and economic costs, compromising the lifespan of other neighboring structures, such as other risers, anchoring systems, and submarine equipment. Therefore, this work aims to study the fall of flexible lazy-wave risers. The influence of the integration algorithm and the time step in the accuracy and efficiency will be studied, as this work deals with the computational modeling of the post-failure phenomenon, focusing at describing an effective way of assessing the fall trajectory, fall time, and the riser accommodation on the seabed. These are important outputs to better understand the fall phenomenon, generating important results aiming at mitigating damage in the case of accidents in future riser projects.

Keywords: Flexible risers, Lazy-wave configuration, Post-failure modeling, Finite Element Analysis.

1 Introduction

Flexible risers are important elements of the offshore industry. Since 1970, these have been used extensively as production and exportation elements, as well as flowlines [1]. These structures present a low bending stiffness, which allows for easier absorption of the platform movement and smoother accommodation on the seabed. However, in harsher environments, the displacements may become too high, imposing a large variation in forces and stresses in a free-hanging catenary. Besides, the free-hanging catenary would be subjected to higher tensile forces at a greater water depth. Thus, in these cases, the lazy-wave configuration is often used. This configuration uses floaters in a delimited section of the riser which lowers the riser top tension and decrease the displacements and stresses variations around the Touchdown Point (TDP) [1].

In a conventional global dynamic analysis, the user often focuses on assessing the maximum top tension and minimum tension and curvature on the TDP [2]. The lazy-wave configuration helps with both of these limits. However, structures are still susceptible to failure during their lifespan, which causes them to fall in the seabed. Post-failure analyses are important to predict the possible fall trajectory, preventing any impact on other structures which would cause them to fail as well [3].

However, very few papers aim at dealing with this type of analysis [4–7], especially regarding flexible risers [8]. Skinner et al. [5] present a study over the fall trajectory of an accidentally dropped drilling riser, developing studies for different bending stiffness in a way to establish a ”safe zone”. Atluri et al. [8] propose the use of a damper capable of reducing the velocity of a falling structure, thus reducing the impact force on the ground or in other structures. It is important to note that post-failure simulations are not easy to perform: due to the abrupt variation in stresses and curvatures, the analysis usually requires a much smaller time step than the conventional nonlinear dynamic analysis.

Thus, this paper aims at studying a variety of parameters that may affect the post-failure simulation to assist in defining the best way to carry out the dynamic analysis after the riser failure. This way, different values for parameters such as bending stiffness, time step and the tangential drag coefficient will be discussed to define an efficient and accurate model for a given simulation. Besides, different nonlinear dynamic algorithms will be tried out, namely the Generalized-α and the Semi-implicit Euler, an implicit and an explicit algorithm, respectively. The results will be given mostly in terms of effective tension, fall trajectory, total kinetic energy, and fall radius. Besides, the deformed configuration during and after the riser fall will be observed.

The rest of the paper is organized as follows. In Section 2 the flexible risers and the lazy-wave configuration are discussed in more detail, as also the hydrodynamic forces and the importance of the tangential drag coefficient for this type of analysis. In Section 3 the post-failure analysis is explained, and the model used is detailed. The results obtained are presented in Section 4 and finally, in Section 5 the main conclusions are brought together.

2 Lazy-wave risers

Flexible risers are characterized by their low bending stiffness. Its usual applications vary from oil transportation between platforms to injection of either gas or water in reservoirs. They easily absorb the movements of the platform and its accommodation on the seabed. These structures are composed of multiple layers that provide impermeability, containment of the internal fluid, and resistance to operational and environmental loads [1]. Understanding which external loads influence a conventional riser analysis is also important to comprehend the post-failure behavior. Self-weight and buoyancy play a big part in this. Those are influenced by, among other things, the material used, dimensions, internal fluid, and, especially in floated sections, the existence of flotation modules. These have a major influence on the behavior of the compressive stress wave right after the failure. Waves and currents can be translated into hydrodynamic forces via the Morrison equations [1]. Since the velocity of the structure can become very high during its fall after the rupture, reaching values greater than 100 km/h, the hydrodynamic forces are very important to the post-failure analysis. Section 2.1 further explores this idea.

Flexible risers can be used in different configurations, the most common being the free-hanging catenary and the lazy-wave. The object of study in this article is a flexible riser in a lazy-wave configuration, as in Figure 1. It is characterized by the existence of floating modules along with its structure in a determined length so that the line assumes the characteristic shape of this configuration [1]. According to Sparks [1], the lazy wave is adopted to reduce the effect of the movements of the vessel on the TDP of the riser. Besides, it allows reducing the stresses in the riser, since it divides the structure into two sections separated by the buoyancy section.

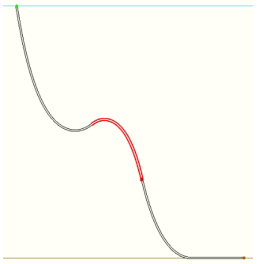

Figure 1. Lazy-wave configuration

2.1 Hydrodynamic forces

On a post-failure analysis, hydrodynamic forces are especially important since the structure can be submitted to high velocities and accelerations. As already pointed out, waves and currents are translated into forces according to the Morison's theory [1], where the hydrodynamic force f_H on submerged cylinders can be evaluated as the sum of the inertia force f_I and the drag force f_D. In the general case, considering the cylinder of volume V in motion, with velocity $\dot{u}$, exposed to flow perpendicular to its longitudinal axis, which moves with an acceleration $\ddot{u}_f$, the hydrodynamic force f_H is given by:

$$f_H = C_M\,\rho\,V\ddot{u}_f - (C_M - 1)\;\rho\,V\ddot{u} + \frac{1}{2}\,\rho\,C_D\,\phi\,(\dot{u}_f - \dot{u})|\dot{u}_f - \dot{u}| \tag{1}$$

where C_M is the inertia coefficient, C_D is the drag coefficient, ρ is the fluid density, and $(\dot{u}_f - \dot{u})$ is the riser relative velocity. In Eq. (1), $C_M - 1$ is usually replaced by the so-called additional mass coefficient C_a.

When the flow is not perpendicular to the riser axis, an approach usually taken is to independently compute hydrodynamic loads in the perpendicular and parallel directions using the cross-flow principle, which establishes that the fluid and structure acceleration vectors can be decomposed into a normal and a tangential direction [1, 9]. On flexible catenary risers, the tangential drag force has a very small contribution. SINTEF [10] shows an experimental study that describes some steps to calculate the tangential drag coefficient so the tangential drag force can be evaluated by:

$$f_t = \frac{1}{2}\,\rho\, C_{Dt}\,\phi\, v_t\,|v_t| \tag{2}$$

where C_{Dt} is the tangential drag coefficient and v_t is the flow velocity in the tangential velocity. SINTEF [10] proposes that, for a flow component perpendicular to the pipe, $C_{Dt} = 0.03\,C_D$ can be a good estimation.

For lazy-wave risers, the tangential drag force is as important as the normal drag force, since there will be a strong interaction between the individual buoyancy elements [11]. As such, the floated section is often submitted to a much higher tangential drag coefficient.

The tangential drag coefficient will be one of the most important parameters discussed in this paper since tangential drag forces are particularly important for long risers with large dynamic axial displacements, which occur during the fall trajectory. Therefore, as this paper focus on the post-failure simulation of lazy-wave risers, a study over the influence of the tangential drag coefficient from both the point of view of the physics of the fall of risers and the numerical aspects of the simulation of this phenomenon will be made.

3 Post-failure analysis

The post-failure analysis is concerned with what happens to a riser after it fails at a given time during the dynamic simulation. In the Finite Element Methods (FEM), this can be done by breaking the connection between two nodes. This abrupt disconnection causes a series of complex events that characterize the behavior of the riser after the rupture [12].

Right after the failure, the effective tension on the breaking node goes to zero, since it is now a free node. This sudden phenomenon triggers compressive stress wave that travels along the line into the fixed end direction. This occurs at both collapsed extremities. Since a riser is a slender structure, small compressive loads can lead to buckling [4]. In conventional analysis, these usually appear on catenary risers near the TDP due to the heave motion of the platform, causing the phenomenon usually known as dynamic buckling [2]. However, the compressive loads that occurs in a post-failure analysis are much larger than the compressive loads induced by the platform movements.

The finite element model must be conceived in a way that it can perform good approximations to the displacement field in a real structure. However, finite elements may suffer from buckling if the compressive loads surpass the critical Euler limit. To correctly capture the riser displacements, the element length l should be small enough to prevent the element buckling [2]. In this paper, l will be set according to the top tension on static analysis T_{top}:

$$P_{cr} = \frac{\pi^2 EI}{l^2} \quad \Rightarrow \quad l = \sqrt{\frac{\pi^2\, EI}{T_{top}}} \tag{3}$$

where EI is the riser bending stiffness.

The post-failure simulation of a riser has similarities with usual structural dynamics and wave propagation problems. As such, it is uncertain whether the better option to use is an implicit or an explicit algorithm. Both will be tested out, and their results will be compared accordingly. A small sensitivity analysis will be performed for different values of EI to understand how the parameter may affect the fall trajectory and final curvatures.

3.1 Model description

The model parameters used in this paper are presented in Table 1. The seabed stiffness was defined as the stiffness which would provide a 2 cm displacement when subjected to a force equals to the structure's apparent weight [13]. Environmental loads (currents and waves) were not considered. The top tension is 1317.3 kN and, by Eq. (3), the element size is set as 0.6 m. A uniform mesh is employed. The structure slenderness is given by $\lambda_s = k\,l/r = 4 \times 10^5$ where $k = 1$, similar to a simply supported beam, l is the total length and $r = \sqrt{EI/EA}$ [13].

In this paper, it is supposed that failure occurs at the end of the buoyant section. In a real case, failure at this point is common due to the existence of corrosion and a high tensile force. The total simulation time considered

Table 1. Model parameters.

Total length (m)	3200	Outer diameter (m)	0.30
Horizontal projection (m)	1800	Inner diameter (m)	0.15
Declination - End A	172.9	Mass per unit length (kg/m)	180
Declination - End B	90	EI (kNm^2)	48
Internal fluid specific weight (kN/m^3)	4	EA (kN)	750000
Distance from top to the buoyant section (m)	1300	GJ (kNm^2)	10
Buoyant section length (m)	700	Added mass coefficient	1.0
Floater diameter (m)	1.6	Normal drag coefficient	1.2
Floater length (m)	3.0	Lateral friction coefficient	1.07
Floater pitch (m)	9.0	Axial friction coefficient	0.35
Floater density (kN/m^3)	6.0	Water depth (m)	2000
Floater added mass coefficient (normal, axial)	1.0, 0.5	Seabed normal stiffness (kN/m/m^2)	217.17
Floater normal drag coefficient	1.2	Seabed shear stiffness (kN/m/m^2)	217.17

was 60 s, which covers the entire riser fall, and the rupture takes place 4 seconds after the simulation starts. Table 2 sums up which parameters will be studied and the values considered in the numerical simulations. Here, a change in λ_s is employed in terms of a change in the bending stiffness EI. The parameters used in the so-called base case are highlighted in bold-face.

Table 2. Model and algorithm parameters studied.

Dynamic algorithm	**Implicit** (Generalized-α) and Explicit (Semi-Implicit Euler)
Time step (s)	0.1, 0.05, **0.01** and 0.005
Cd_t	0.00, **0.01**, 0.02 and 0.03
λ_s	$\mathbf{4 \times 10^5}$, 2×10^5, 1×10^5 and 5×10^4

Results will be shown in terms of the deformed configuration during the fall, geometry in the seabed, compressive load wave, and total kinetic energy. Besides, some simulation parameters such as the wall-clock time (WCT), the total number of iterations (N_{it}), and the fall time will be discussed (t_f). The fall radius (R_f) is another important parameter, which, in this paper, is given by the maximum distance between a node and the TDP position (evaluated from the static analysis). All analyses will be performed using the OrcaFlex software, on a computer with a core i9-9820X CPU of 3.30 GHz clock speed and 128 GB of RAM. It is worth noting that, on OrcaFlex, a multiplication by π is introduced in Eq. (2) [9]. Thus, to maintain equivalence, values for C_{Dt} should be divided by π before set in the program.

4 Results and discussion

Table 3 presents the results found in most analyses conducted. Given the complexity of the phenomenon, it is not easy to complete a simulation, especially with larger time steps: with $\lambda_s = 4 \times 10^5$ it was not possible to conclude the simulation using time steps of 0.050 s and 0.100 s. However, both an increase in C_{Dt} and a decrease in slenderness simplify the analysis, as both WCT and N_{it} decrease. Furthermore, for $\lambda_s = 5 \times 10^4$ the simulation can be concluded for all time steps. However, since more iterations per step are needed when increasing the time step, the lower WCT is achieved with a time step of 0.050 s.

One explanation for faster analysis when reducing the slenderness is that the stiffness matrix might become ill-conditioned when some of its members (related to the bending stiffness EI) are much smaller than the others (related to the axial stiffness EA). In that case, a hybrid element formulation could be of great assistance to the analysis convergence [13]. Regarding the C_{Dt}, it is noted a major influence on the fall time t_f. Moreover, there is initially a clear increase in the fall radius R_f, which is then smoothed out for higher values of C_{Dt}. It is important to note that a lower λ_s also causes an increase in R_f.

The results found using the explicit algorithm were close to results from the implicit case. However, the WCT was up to 8 times longer. This implies that the explicit approach might not be advantageous in this situation.

Figure 2 shows a time-lapse to present the configuration during the fall. While the upper section slowly goes up, due to the existence of buoyancy modules, the lower section falls in a much higher velocity, also presenting much greater curvatures. This is the critical section for this type of analysis. While at the beginning of the

Table 3. Non-linear dynamic analysis results.

Time step (s)	C_{Dt}	λ_s ($\times 10^5$)	Algorithm	WCT (min)	t_f (s)	R_f (m)	N_{it}	$\overline{N}_{it}$
0.005	0	4.00	Implicit	43	32	191.71	22586	1.88
	0.01	4.00		-	-	-	-	-
	0.02	4.00		30	47	245.28	13387	1.12
	0.03	4.00		30	55	246.57	12680	1.06
0.010	0	4.00		-	-	-	-	-
	0.01	4.00		33	40	216.53	13799	2.30
	0.02	4.00		27	47	261.84	11087	1.85
	0.03	4.00		24	53	260.89	9367	1.56
Default	0	4.00	Explicit	194	31	217.43	-	-
	0.01	4.00		201	39	254.02	-	-
	0.02	4.00		200	47	243.95	-	-
	0.03	4.00		200	53	254.15	-	-
0.010	0.01	4.00	Implicit	32	40	216.53	13799	2.30
		2.00		22	40	219.38	8227	1.37
		1.00		18	35	221.28	6372	1.06
		0.50		17	35	236.17	6014	1.00
0.050		0.50		5	52	239.54	2802	2.33
0.100		0.50		8	56	294.89	3150	5.24

simulation buckling occurs mainly closer to the TDP, the phenomenon spreads quickly to the rest of the riser, until it reaches the free end.

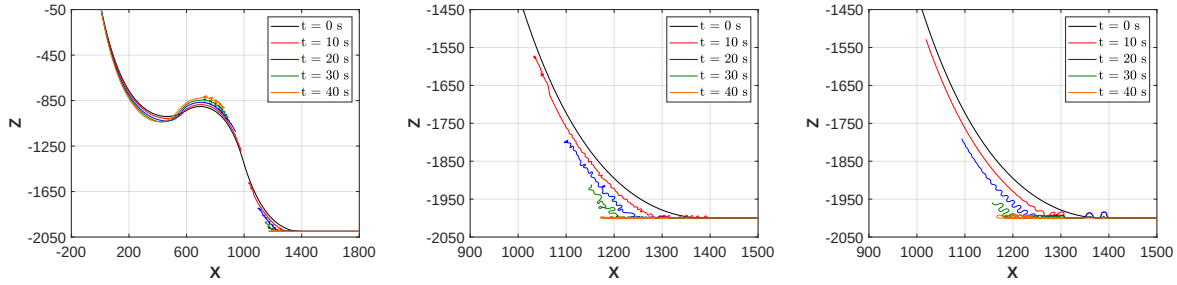

(a) Entire structure (b) Zoom-in on the falling section (c) Zoom-in with $\lambda_s = 1 \times 10^5$

Figure 2. Deformed configuration during the fall

Figure 3 presents the compressive load wave right after the riser failure for implicit and explicit algorithms. Here, it is possible to note a clear difference between algorithms, mainly after the reflection at the anchor point, which happens in approximately 0.58 s, according to riser celerity ($c = 2041.24$ m/s). Thereafter, the compressive wave behavior becomes more complex and more difficult to represent for the two algorithms. However, some important aspects do remain the same (e.g. maximum compression close to 800 kN and speed of the compression wave). It is important to note that there is a slight wave reflection, along with refraction, at the TDP (2785 m). This occurs due to the abrupt increase in stiffness due to the riser-soil interaction.

Figure 4 shows the the final riser configuration at the seabed for different λ_s. The effect of the riser slenderness is noticeable in the results. The reduction of slenderness leads to lower curvatures, fewer loops, and a greater R_f. It is important to note that, in a real case, the consideration of a nonlinear moment-curvature relationship may have a large influence on the final configuration [14].

Finally, Figure 5 shows the total kinetic energy of the falling section over time, after the rupture. As expected, the algorithm used does not influence this parameter, while the slenderness λ_s slightly affects the result. However, even small variations in the C_{Dt} lead to very different results. This parameter is usually ignored in usual analyses, since tangential loads are not common except for the buoyant section [11], but this parameter seems to be very important in this type of analysis.

The peak of kinetic energy occurs around 10 seconds after the failure. From there, the total kinetic energy starts to fall due to two factors: dissipative forces (Morrison forces) and the continuous decrease in the falling length throughout the simulation. The total kinetic energy reaches 0 exactly at the fall time t_f.

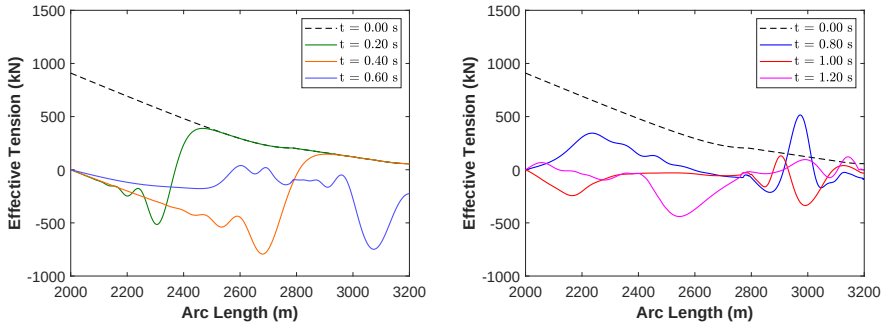

(a) Before reflection, on a Implicit Algorithm (b) After reflection, on a Implicit Algorithm

(c) Before reflection, on a Explicit Algorithm (d) After reflection, on a Explicit Algorithm

Figure 3. Compressive load wave behavior right after the rupture in the falling section.

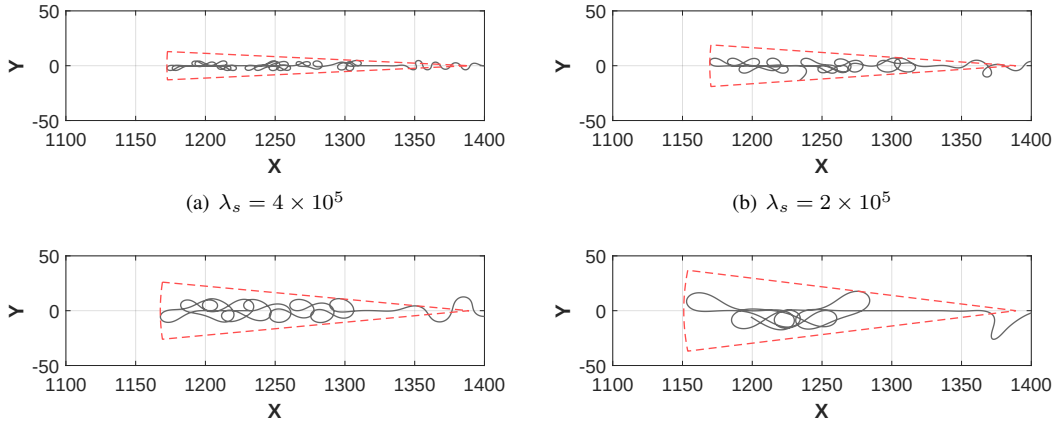

(a) $\lambda_s = 4 \times 10^5$ (b) $\lambda_s = 2 \times 10^5$

(c) $\lambda_s = 1 \times 10^5$ (d) $\lambda_s = 5 \times 10^4$

Figure 4. Final soil configuration after the riser fall.

5 Conclusion

This paper addresses the nonlinear dynamic analysis of a falling lazy-wave riser after failure. The influence of key parameters, such as the time step, dynamic algorithm, C_{Dt}, and slenderness, is discussed.

The use of the implicit algorithm was seen to be more advantageous since the algorithm type did not seem to have a very large influence on most results, although the wall-clock time with the explicit algorithm can be up to 8 times greater than the time spent with the implicit algorithm.

Increasing C_{Dt} eases out (lower total number of iterations) and speeds up (lower WCT) the simulation, while also usually leading to an increase in the fall radius R_f and the fall time t_f.

On the other hand, increasing the riser slenderness (λ_s) seems to make the analysis more difficult, requiring smaller time steps in order to complete the simulation. This parameter also heavily influences the formation of loops and curvatures during the fall, as lower values of λ_s implies in greater curvatures and greater R_f.

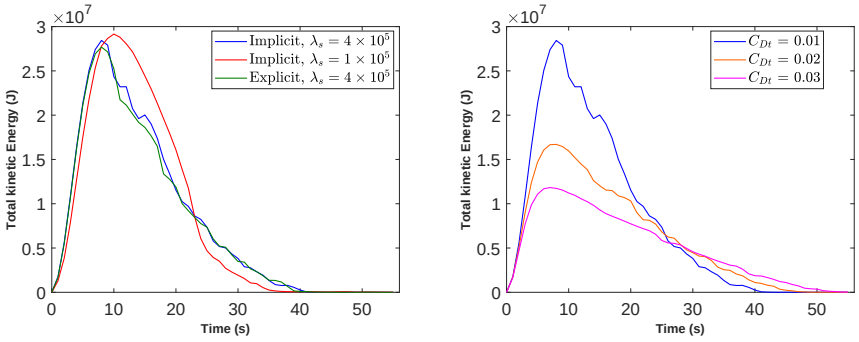

(a) Comparison between different algorithms and λ_s (b) Comparison between different C_{Dt}

Figure 5. Total kinetic energy in the falling section during the analysis.

The procedure described in this paper can be used to evaluate the risk of clashing between the falling riser and neighboring structures on future works.

Acknowledgements

The authors gratefully acknowledge Petrobras and CNPq (Conselho Nacional de Desenvolvimento Científico e Tecnológico) for the financial support.

Authorship statement. The authors hereby confirm that they are the sole liable persons responsible for the authorship of this work, and that all material that has been herein included as part of the present paper is either the property (and authorship) of the authors, or has the permission of the owners to be included here.

References

[1] Sparks, C. P., 2007. *Fundamentals of marine riser mechanics: basic principles and simplified analyses*. Penn Well.

[2] Ribeiro, E., Roveri, F., & Mourelle, M., 1998. Dynamic compression buckling in flexible riser. *Offshore Technology Conference*.

[3] Gao, Q., Duan, M., Liu, X., Wang, Y., Jia, X., An, C., & Zhang, T., 2018. Damage assessment for submarine photoelectric composite cable under anchor impact. *Applied Ocean Research*, vol. 73, pp. 42–58.

[4] Pestana, R. G., Roveri, F. E., Franciss, R., & Ellwanger, G. B., 2016. Marine riser emergency disconnection analysis using scalar elements for tensioner modelling. *Applied Ocean Research*, vol. 59, pp. 83–92.

[5] Skinner, B., Wadhwa, H., & Majed, A., 2018. Collapse simulation of an accidentally dropped drill riser. *28th International Ocean and Polar Engineering Conference*.

[6] Meng, S., Che, C., & Zhang, W., 2018. Discharging flow effect on the recoil response of a deep-water drilling riser after an emergency disconnect. *Ocean Engineering*, vol. 151, pp. 199–205.

[7] Wang, Y. & Gao, D., 2019. Recoil analysis of deepwater drilling riser after emergency disconnection. *Ocean Engineering*, vol. 189, pp. 106406.

[8] Atluri, S., Liu, N., Sablok, A., & Weaver, T., 2010. Dynamic analysis of riser release and lowering. *29th International Conference on Ocean, Offshore and Arctic Engineering: Volume 6*.

[9] Orcina, 2020. Orcaflex user's manual.
`www.orcina.com/webhelp/OrcaFlex/Default.htm`.

[10] SINTEF, 2017. Handbook on design and operation of flexible pipes.
`www.sintef.no/en/ocean/handbook-on-design-and-operation-of-flexible-pipes/`.

[11] Det Norske Veritas, 2010. Dnv-os-f201, dynamic risers.
`rules.dnvgl.com/docs/pdf/DNV/codes/docs/2010-10/Os-F201`.

[12] Paredes, M., Wierzbicki, T., & Roth, C. C., 2015. Three dimensional, flexural-torsional dynamic buckling of long wires after tensile fracture and implications on deep water riser dynamics. *International Journal of Impact Engineering*, vol. 86, pp. 27–39.

[13] Junior, D. L. K., 2003. Análise dinâmica de linhas flexíveis com elemento de pórtico não-linear geométrico híbrido. Master's thesis, Universidade Federal do Rio de Janeiro.

[14] Coyne, J., 1990. Analysis of the formation and elimination of loops in twisted cable. *IEEE Journal of Oceanic Engineering*, vol. 15, n. 2, pp. 72–83.